

First principles elastic constants and electronic structure of α -Pt₂Si and PtSi

O. Beckstein,⁽¹⁾ J. E. Klepeis,⁽²⁾ G. L. W. Hart,⁽³⁾ and O. Pankratov⁽¹⁾

⁽¹⁾ *University of Erlangen-Nürnberg, Erlangen, Germany D-91058*

⁽²⁾ *Lawrence Livermore National Laboratory, University of California, Livermore, CA 94551*

⁽³⁾ *National Renewable Energy Laboratory, Golden CO 80401*

(15 March 2001)

We have carried out a first principles study of the elastic properties and electronic structure for two room-temperature stable Pt silicide phases, tetragonal α -Pt₂Si and orthorhombic PtSi. We have calculated all of the equilibrium structural parameters for both phases: the a and c lattice constants for α -Pt₂Si and the a , b , and c lattice constants and four internal structural parameters for PtSi. These results agree closely with experimental data. We have also calculated the zero-pressure elastic constants, confirming prior results for pure Pt and Si and predicting values for the six (nine) independent, non-zero elastic constants of α -Pt₂Si (PtSi). These calculations include a full treatment of all relevant internal displacements induced by the elastic strains, including an explicit determination of the dimensionless internal displacement parameters for the three strains in α -Pt₂Si for which they are non-zero. We have analyzed the trends in the calculated elastic constants, both within a given material as well as between the two silicides and the pure Pt and Si phases. The calculated electronic structure confirms that the two silicides are poor metals with a low density of states at the Fermi level, and consequently we expect that the Drude component of the optical absorption will be much smaller than in good metals such as pure Pt. This observation, combined with the topology found in the first principles spin-orbit split band structure, suggests that it may be important to include the interband contribution to the optical absorption, even in the infrared region.

PACS 62.20.Dc, 71.20.Be, 71.15.Nc

I. INTRODUCTION

Metallic Pt silicide compounds are used to make rectifying junctions on silicon substrates. The Schottky barrier, which determines the activation energy for transport of the charge carriers (holes), is 220–240 meV for orthorhombic PtSi on p-type Si(001),^{1,2} matching an important atmospheric “transparency window” in the infrared region. For this reason these materials are well suited to infrared detector applications. Orthorhombic IrSi has also been used in these applications and has a Schottky barrier of 160 meV on Si(001),³ matching a lower portion of the transparency window. An important advantage of the silicides is that they are more compatible with current silicon-based fabrication technology than infrared sensitive semiconductors such as InSb and Hg_xCd_{1-x}Te.

Despite their importance in infrared detector applications, relatively little theoretical work has been done to investigate the fundamental electronic structure and equilibrium properties of the Pt silicides. Bisi *et al.*⁴ used the iterative extended Huckel method to calculate the angular-momentum-resolved density of states (DOS) for a number of near noble-metal silicides, including α -Pt₂Si and PtSi. Yarmoshenko *et al.*⁵ compared x-ray photoelectron spectroscopy (XPS) and x-ray emission spectroscopy (XES) measurements to the electronic structure calculated using a linear muffin-tin orbital (LMTO) method for a number of 4d and 5d silicides, including PtSi. In order to provide a more complete understand-

ing of the properties of the Pt silicides we have carried out first principles electronic structure calculations for two room-temperature stable phases, tetragonal α -Pt₂Si and orthorhombic PtSi. In addition to calculating all of the equilibrium structural parameters (Sec. II) we have also obtained values for all of the zero-pressure elastic constants (Sec. III) for both phases. We have investigated the electronic structure (Sec. IV) which is directly relevant to the infrared detector applications of these materials. The purpose in all of these calculations has been to provide a fundamental understanding of the ground state properties of the Pt silicides. We summarize our results in Sec. V.

II. ATOMIC STRUCTURE

A. Crystal structures

Table I summarizes the characteristics of the equilibrium crystal structures for each of the materials considered here. The pure Pt and Si constituents of the Pt silicides both crystallize in a cubic structure under normal conditions, face-centered cubic (fcc) for Pt⁶ and cubic diamond for Si.⁷ Both cubic structures are characterized by a single lattice constant a (Table II).

The conventional unit cells of the two Pt silicides α -Pt₂Si and PtSi are illustrated in Fig. 1. The structure of the room-temperature ($T < 968$ K) α -phase of Pt₂Si is body-centered tetragonal (bct) and resembles a distorted

CaF₂ structure.^{8,9} A central Si atom is surrounded by eight Pt atoms, which are located in the corners of a rectangular cell elongated along the *c*-axis. There are two symmetry-equivalent Pt and one Si atom in the primitive cell. The unit cell is characterized by two lattice constants *a* and *c* (Table II).

PtSi has a primitive orthorhombic structure [see Fig. 1(b)] with four symmetry-equivalent Pt and four symmetry-equivalent Si atoms per primitive cell in an MnP-type lattice.^{10,11} This structure is characterized by three lattice constants, denoted *a*, *b*, and *c* (Table II). Half of the Pt and half of the Si atoms in the primitive cell are located in a (010) plane at $\frac{1}{4}b$ with the rest of the atoms in a (010) plane at $\frac{3}{4}b$. The in-plane atomic coordinates are not completely specified by the space group symmetry and thus there are four free internal structural parameters u_{Pt} , v_{Pt} , u_{Si} , and v_{Si} (the “1st position” column in Table I). The experimental values are given in Table III. Each Si is surrounded by six Pt atoms at the corners of a distorted trigonal prism. The Pt atoms have six Si neighbors at the corners of a distorted octahedron, and four Pt neighbors, which are positioned in four of the octahedral interstices.¹¹ The Pt atoms are arranged in zig-zag chains along the [100] direction.

B. FPLMTO method

The equilibrium structural parameters and zero-pressure elastic constants were calculated with a full potential linear muffin-tin orbital (FPLMTO) method^{12,13} which makes no shape approximation for the crystal potential. For mathematical convenience the crystal is divided into regions inside atomic spheres, where Schrödinger’s equation is solved numerically, and an interstitial region. In our FPLMTO method the basis functions in the interstitial region are smoothed Hankel functions.¹⁴ This method does *not* require the use of empty spheres, even for open structures such as cubic-diamond-phase Si. The atoms were treated scalar relativistically within the local density approximation, using the exchange-correlation potential of Ceperley and Alder.¹⁵ Spin-orbit interactions were not included. The choice of basis functions for the Pt and Si atoms was optimized according to the procedure described in Ref. 12. The parameters describing the basis are listed in Table IV and were used in the calculations for both silicides in addition to pure Pt and pure Si.¹⁶ The Si 3*s*, 3*p*, 3*d*, and 4*f* as well as the Pt 6*s*, 6*p*, 5*d*, and 5*f* were all included as valence orbitals. The Pt semi-core 5*s* and 5*p* were treated as core orbitals and we have not used the frozen overlapped core approximation (FOCA—see Ref. 12).

The equilibrium volume V_0 and bulk modulus B_0 of Pt and Si were determined by fitting the total energy calculated at nine different lattice constants to a Murnaghan equation of state.^{17,18} In the case of Pt (Si) we used a $24 \times 24 \times 24$ ($12 \times 12 \times 12$) cubic special *k*-point mesh which

gave 6912 (864) points in the full Brillouin zone (BZ) and 182 (28) points in the irreducible wedge. In addition, a real space mesh is used for calculating integrals of the potential over the interstitial region. We used a $16 \times 16 \times 16$ mesh for Pt and an $18 \times 18 \times 18$ mesh for Si. With these choices the total energies were converged to better than 1 μRy per atom.

In order to determine the equilibrium lattice constants of the silicides, the total energy hypersurfaces were minimized simultaneously with respect to all of the lattice parameters. In the case of tetragonal $\alpha\text{-Pt}_2\text{Si}$, total-energy calculations were performed at nine different values of each of the two lattice constants *a* and *c* (a total of 81 calculations) in the range $0.93 \leq a/a_{\text{exp}}$, $c/c_{\text{exp}} \leq 1.07$. For orthorhombic PtSi we used seven different values of *a*, *b*, and *c*, respectively (343 calculations), within the same relative ranges. For both $\alpha\text{-Pt}_2\text{Si}$ and PtSi, 216 *k*-points were sampled in the full BZ which reduced to 28 and 27 special *k*-points in the irreducible wedge, respectively. In the case of $\alpha\text{-Pt}_2\text{Si}$ a $16 \times 16 \times 16$ real space mesh was used for the interstitial integrals and a $24 \times 16 \times 24$ mesh was used for PtSi. With these choices the energy per atom differed from the fully converged value (which was found for approximately 13 000 *k*-points in the full BZ) by 0.20 mRy for $\alpha\text{-Pt}_2\text{Si}$ and 0.19 mRy for PtSi. The resulting total energy hypersurfaces, $E(a, c)$ and $E(a, b, c)$, were each fit to a third order polynomial in the lattice parameters. These polynomials were then minimized to yield the equilibrium parameters. The bulk modulus and equilibrium volume were obtained by fitting the total energy as a function of volume to a four-term Birch-Murnaghan equation of state,¹⁹

$$E(V) = \sum_{n=1}^4 a_n V^{-2n/3}. \quad (1)$$

This fit was differentiated twice, yielding the bulk modulus $B_0 = V \left[\frac{\partial^2 E(V)}{\partial V^2} \right]_{V_0}$ at the theoretical equilibrium volume.

The four free internal structural parameters of orthorhombic PtSi, (u_{Pt} , v_{Pt} , u_{Si} and v_{Si} in Table I), were determined self-consistently by calculating the *ab initio* forces^{12,20} on the ions and, within the Born-Oppenheimer approximation,²¹ relaxing the position of each individual atom in the direction of the forces until the absolute values of the forces were converged to less than 1.5 mRy/a.u. 512 special *k*-points were used within the full BZ (corresponding to 64 in the irreducible wedge). Initially the atomic positions were relaxed starting from the experimental structure¹¹ and holding the three lattice constants fixed at their experimental values. Using these theoretically determined internal parameters, the theoretical equilibrium lattice constants, a_0 , b_0 , and c_0 , as well as the bulk modulus B_0 , were determined using the procedure described above. A second geometry relaxation was then carried out but now holding the lattice constants fixed at these theoretically determined equilibrium values. This

yielded a second set of internal structural parameters which we refer to as the self-consistent theoretical values. In principle this cycle could be repeated many times to obtain a set of lattice constants and internal parameters which are truly “self-consistent.”²² However, in practice we find that after the first cycle there are only small differences between the two sets of internal parameters (see Table III) and so we regard them as being converged. We also note that the value of B_0 obtained using fixed values of the internal structural parameters, as described here, is not strictly correct and that we relax the constraint of fixed internal parameters when we discuss the elastic constants (including B_0) in Sec. III E.

C. Equilibrium properties

In order to test our method¹² and, in particular, to test our choice of basis functions, we calculated the equilibrium lattice constant a_0 and bulk modulus B_0 for Pt and Si as described in Sec. II B. The results are given in Table II and compared to experimental data. Since we will focus next on the elastic constants, we pay particular attention to B_0 , which is essentially an elastic constant. We see in Table II that we obtain rather good agreement between our values and the experimental data. The self-consistent equilibrium lattice-constants a_0 and c_0 for α -Pt₂Si are also listed in Table II, along with the theoretical a_0 , b_0 , and c_0 lattice constants for PtSi. The bulk moduli B_0 at the theoretical volumes for both Pt silicides are also given.

In Table III we list the internal structural parameters for PtSi. The values calculated using the experimental lattice constants are very close to those measured by Graeber *et al.*¹¹ Comparing the atomic positions using the experimental versus the theoretical internal parameters, we find absolute shifts in the positions of less than 0.028 a.u. The self-consistent internal parameters obtained using the theoretical lattice constants are generally even closer to the experimental values. In this case the absolute atomic shifts relative to the experimental geometry are less than 0.023 a.u.

The theoretical cohesive energies E_{coh} and heats of formation ΔH_f for the self-consistent equilibrium atomic geometries are compared to the experimental values in Table V. As is typically the case, our local-density-functional based calculations overestimate the cohesive energy. However, the calculated heats of formation are much closer to the experiment. The experimental heats of formation are given for $T = 298.15$ K whereas the theoretical values correspond to 0 K and do not include corrections for zero-point vibrations. We note that the heats of formation are very similar for the two silicides and that a plot of the theoretical ΔH_f as a function of atomic percent Pt is concave up, as required for the silicides to both be thermodynamically stable.

III. ELASTIC CONSTANTS

A. Method of calculation

The elastic constants determine the stiffness of a crystal against an externally applied strain. For small deformations we expect a quadratic dependence of the crystal energy E on the strain (Hooke’s law). The elastic constants c_{ijkl} describe this quadratic behavior. Consider a displacement $\mathbf{u}(\mathbf{R})$ which takes every Bravais lattice point \mathbf{R} of the undistorted lattice to a new position \mathbf{R}' in the strained lattice,

$$\mathbf{R}'_i = R_i + u_i(\mathbf{R}), \quad (2)$$

where the index i corresponds to Cartesian coordinates. If we assume the applied strain is homogeneous (uniform throughout the crystal), we can rewrite Eq. 2 as

$$\mathbf{R}'_i = \sum_j \alpha_{ij} R_j \quad \text{with} \quad \alpha_{ij} = \delta_{ij} + \frac{\partial u_i(\mathbf{R})}{\partial R_j}. \quad (3)$$

For a homogeneous applied strain the displacement gradients $\partial u_i(\mathbf{R})/\partial R_j$ are simply constants, independent of \mathbf{R} . These displacement gradients define the nine components of a tensor. However, since the total energy E cannot change under rotations of the crystal as a whole, E can only depend on the symmetric part of the deformation,²³ called the strain tensor ϵ :

$$\epsilon_{ij} = \frac{1}{2} \left[\frac{\partial u_i(\mathbf{R})}{\partial R_j} + \frac{\partial u_j(\mathbf{R})}{\partial R_i} \right]. \quad (4)$$

Expanding the internal energy $E(V, \epsilon)$ of the crystal with respect to the strain tensor gives²⁴

$$E(V, \{\epsilon_{mn}\}) = E(V) + V \sum_{ij} \sigma_{ij} \epsilon_{ij} + \frac{V}{2} \sum_{ijkl} c_{ijkl} \epsilon_{ij} \epsilon_{kl} + \dots, \quad (5)$$

where the stress tensor σ is defined by

$$\sigma_{ij} = \frac{1}{V} \left[\frac{\partial E(V, \{\epsilon_{mn}\})}{\partial \epsilon_{ij}} \right]_{\epsilon=0}, \quad (6)$$

the second order adiabatic elastic constants are given by

$$c_{ijkl} = \frac{1}{V} \left[\frac{\partial^2 E(V, \{\epsilon_{mn}\})}{\partial \epsilon_{ij} \partial \epsilon_{kl}} \right]_{\epsilon=0}, \quad (7)$$

and V is the volume of the unstrained crystal. It is convenient to use Voigt notation which takes advantage of the symmetries of the tensors: $xx \rightarrow 1$, $yy \rightarrow 2$, $zz \rightarrow 3$, $yz \rightarrow 4$, $xz \rightarrow 5$ and $xy \rightarrow 6$. Using this notation Eq. (5) becomes²³

$$E(V, \{e_i\}) = E(V) + V \sum_i \sigma_i e_i + \frac{V}{2} \sum_{ij} c_{ij} e_i e_j + \dots \quad (8)$$

with the strain tensor given by

$$\epsilon = \begin{pmatrix} e_1 & \frac{1}{2}e_6 & \frac{1}{2}e_5 \\ \frac{1}{2}e_6 & e_2 & \frac{1}{2}e_4 \\ \frac{1}{2}e_5 & \frac{1}{2}e_4 & e_3 \end{pmatrix}. \quad (9)$$

In order to calculate all M elastic constants of a crystal we applied M independent strains $\epsilon^{(I)}$ to the unit cell, using Eqs. (3) and (4) to determine the atom positions within the strained unit cell. In particular, we have $M = 3$ for both cubic Si and cubic Pt, $M = 6$ for tetragonal Pt₂Si, and $M = 9$ for orthorhombic PtSi. Each strain $I = 1, \dots, M$ was parameterized by a single variable γ and we calculated the total energy $E^{(I)}(\gamma)$ for a number of small values of γ . For these small distortions, $E^{(I)}(\gamma)$ was fit to a polynomial in γ and then equated to the appropriate elastic constant expression $E(V, \{e_i^{(I)}(\gamma)\})$ in Eq. (8). From all of the fits we obtained a system of M linear equations for the elastic constants, which was solved for the c_{ij} . Since we always take the undistorted crystal to be the zero-pressure theoretical equilibrium structure, the applied stress σ is zero and so the second term of Eqs. (5) and (8) does not enter in the calculations described here.

The parameterizations we used for the three independent strains in the cubic cases of Pt and Si are given in Table VI. Strain $I = 1$ is a volume-conserving stretch along the \mathbf{z} -axis, the second strain is equivalent to simple hydrostatic pressure, and strain $I = 3$ corresponds to a volume-conserving monoclinic shear about the \mathbf{z} -axis. We carried out calculations for 9 values of γ in the range of -0.01 to 0.01 for strains 1 and 2. However, for strain 3 we calculated 9 points in the range from -0.04 to 0.04 because the changes in the energy were rather small (a maximum of 0.1 mRy for $\gamma = 0.01$), leading to larger error estimates in the case of the smaller range. In order to calculate the six independent and non-vanishing elastic constants of tetragonal α -Pt₂Si we used the strains given in Table VII.²⁶ Orthorhombic PtSi has nine independent elastic constants and we chose the nine strains listed in Table VIII. For each of the silicide strains we carried out calculations for seven values of γ in the range of -0.01 to 0.01 , except for strains 8 and 9 in the case of PtSi where only five values of γ were considered (these monoclinic strains were particularly CPU intensive). Computational errors in the elastic constants were determined from the least-squares fit to $E(\gamma)$. All of our results were obtained from fits of the energy to third order in γ because these yielded the smallest errors compared to polynomials of order two and four; the single exception was Pt c_{44} , where minimum standard errors resulted from a fourth order fit.

Calculations of the elastic constants require a very high degree of precision because the energy differences involved are of the order of 10 to 1000 μ Ry. This circumstance requires the use of a fine \mathbf{k} -point mesh. With our choice of $23\,328$ special \mathbf{k} -points in the full BZ for Pt, 864 for Si, and 5832 for α -Pt₂Si and PtSi, the en-

ergy per atom was converged to $1\,\mu$ Ry or better in all cases. In order to minimize numerical uncertainties we used the same \mathbf{k} -point mesh for all of the calculations in a given material. The differing symmetries of the various strains I resulted in differing numbers of irreducible \mathbf{k} -points. We also checked that we obtained the same total energy for $\gamma = 0$, regardless of strain I (and hence different symmetry and irreducible \mathbf{k} -points). All of the calculations were carried out at the theoretical equilibrium lattice constants listed in Table II. Relaxation of the internal degrees of freedom was carried out in the case of all nine PtSi elastic constants. These relaxations are necessary because the atomic positions are not completely fixed by the space group symmetry, even for the unstrained crystal, and consequently there exist free internal parameters (see Table III) which must be re-determined for any distortion of the crystal, including hydrostatic pressure. Relaxations were also carried out in those cases where the strain-induced symmetry-reduction prompted it (c_{44} for Si and strains 1, 4, 6 for α -Pt₂Si). For comparison we have calculated “frozen” elastic constants in these same cases, where the internal structural parameters were frozen at their zero-strain equilibrium values.

B. Pt

The three elastic constants for Pt are listed in Table IX. Pt is the only one of the metals considered in this work for which experimental data on elasticity is available. MacFarlane *et al.*²⁸ extrapolated the values to 0 K, which makes them well suited for a comparison to our zero-temperature calculations. In the case of c_{11} and c_{12} we find good agreement between our results and the experimental data (within 3–4%). The value of c_{44} deviates by 14%, although the absolute error is approximately 10 GPa for all three elastic constants. The error in c_{44} can be understood if we look closely at the band structure. Pt exhibits a wealth of van Hove singularities directly at the Fermi energy, making it difficult to integrate over the Fermi surface. A high density of \mathbf{k} -points ($23\,328$ in the full BZ) and a very small smearing width of 7 mRy in the higher-order smearing procedure²⁹ are essential because the Fermi energy and hence the total energy depend quite sensitively on these parameters. The calculated value of c_{44} was found to be more sensitive to the \mathbf{k} -points than the other two elastic constants. Conversely, the silicides did not warrant such a special treatment and were calculated with a smearing width of 25 mRy. It seems plausible that a more accurate treatment of the elastic properties of Pt may also require inclusion of spin-orbit coupling. The bulk modulus calculated from the theoretical values of the elastic constants [$B_0 = \frac{1}{3}(c_{11} + 2c_{12})$] is 290.8 GPa. It agrees well with both the experimental value of 288.4 GPa and the one extracted from the fit to a Murnaghan equation of state,

287.8 GPa (Sec. II C).

The requirement of mechanical stability in a cubic crystal leads to the following restrictions on the elastic constants²⁴

$$(c_{11} - c_{12}) > 0, \quad c_{11} > 0 \quad c_{44} > 0, \quad (c_{11} + 2c_{12}) > 0. \quad (10)$$

The Pt elastic constants in Table IX obey these stability conditions, including the fact that c_{12} must be smaller than c_{11} . These conditions also lead to a restriction on the magnitude of B_0 . Since B_0 is a weighted average of c_{11} and c_{12} and stability requires that c_{12} be smaller than c_{11} , we are left with the result that B_0 is required to be intermediate in value between c_{11} and c_{12} ,

$$c_{12} < B_0 < c_{11}. \quad (11)$$

C. Si

Because Si has a cubic structure, it has only three distinct, non-vanishing elastic constants. These were determined with the same strains as in the case of Pt (Table VI). Our results are close to experiment, as indicated in Table IX. The bulk moduli from the total energy minimization and from the elastic constants [$B_0 = \frac{1}{3}(c_{11} + 2c_{12})$] have the same value of 95.9 GPa, close to the one calculated from the experimental elastic constants, 97.0 GPa. The Si elastic constants in Table IX also obey the cubic stability conditions in Eq. (10), meaning that $c_{12} < B_0 < c_{11}$.

It is perhaps worth noting that the calculation of c_{44} required a relaxation of the positions of the Si atoms within the distorted unit cell. The symmetry reduction by the monoclinic shear ($\epsilon^{(3)}$ in Table VI) allowed the Si atoms to relax in the [001] direction. Without this relaxation, c_{44} would have been 108.6 GPa; this is to be compared with the relaxed value of 79.9 GPa and the experimental value of 79.1 GPa.³⁰ We have also obtained the dimensionless Kleinman internal displacement parameter ζ which determines the magnitude of the internal displacements along the [001] direction,

$$\Delta u_3^{(I=3)} = \zeta \frac{a}{4} \epsilon_{xy}, \quad (12)$$

where a is the lattice constant and $\epsilon_{xy} = \frac{1}{2}e_6$ is the appropriate element of the strain tensor [Eq. (9) and Table VI]. Fitting our calculated values of $\Delta u_3^{(I=3)}$ to a quadratic function in γ we find a value of $\zeta = 0.53$ which agrees very well with the experimental value of 0.54.³¹

D. α -Pt₂Si

We have applied the six strains listed in Table VII in order to determine the elastic constants of tetragonal α -Pt₂Si. The orthorhombic strains 1 and 4, and the monoclinic strain 6 all reduce the symmetry of the crystal

in such a way that the positions of the Pt atoms are no longer completely fixed by the symmetry. The strain-induced forces drive them into energetically more favorable positions. However, the Si atom occupies a center of inversion symmetry and thus Si internal displacements are forbidden in all cases (i.e. the strain-induced forces are identically zero). Symmetry also places specific restrictions on the nature of the Pt displacements. The symmetry of strain 6, corresponding to c_{44} , allows Pt internal displacements along both the [010] and [001] directions, while the inversion operation leads to the requirement that the displacements must be equal and opposite for the two Pt atoms in the primitive cell. The symmetry of strain 4, corresponding to c_{11} , is the same as the symmetry of strain 1 and both allow internal displacements only along [001]. Once again the presence of inversion requires that the displacements of the two Pt atoms be equal and opposite. Strain 5, corresponding to c_{33} , and strain 2 result in the same symmetry as the unstrained crystal and therefore there are no internal displacements associated with these cases, since there are no degrees of freedom in the internal atomic coordinates of the unstrained crystal. Strain 3 does lower the symmetry but internal displacements are still symmetry-forbidden. This fact, combined with the lack of displacements associated with strain 2 means that c_{66} is unaffected. We note that since strains 1 and 4 result in the same symmetry reduction relative to the unstrained crystal there will necessarily be a formal symmetry-required relationship between the internal displacements for these two strains. This relationship is obtained directly from the first principles calculations.

In addition to placing restrictions on the nature of the internal displacements, symmetry also constrains the corresponding changes in the elastic constants themselves. We have already seen that the values of c_{11} and c_{44} are both allowed to change as a result of internal displacements but that c_{33} and c_{66} must both remain unchanged. The bulk modulus B_0 is also required to be unchanged because it represents the crystal response to hydrostatic pressure, corresponding to a strain $\epsilon^{(B)} = \gamma \delta_{ij}$ which preserves the full symmetry of the unstrained crystal, just as in the case of strains 2 and 5. The expression for the bulk modulus in terms of the elastic constants is $B_0 = \frac{1}{9}(2c_{11} + c_{33} + 2c_{12} + 4c_{13})$ while the energy expression corresponding to strain 2 is $(c_{11} + c_{12} - 4c_{13} + 2c_{33})\gamma^2$ (see Table VII). Our symmetry arguments have required that neither of these expressions can change as a result of internal displacements and therefore the changes in c_{11} , c_{12} , and c_{13} must exactly cancel from these two expressions (we have already shown in conjunction with strain 5 that c_{33} cannot change). The only way to achieve both cancellations is if the displacement-induced change in c_{13} is identically zero and if the changes in c_{11} and c_{12} are equal and opposite. Moreover, since c_{11} appears as the sole coefficient in the energy expression corresponding to

strain 4 and since internal displacements can only lower the energy, we conclude that the value of c_{11} must either decrease or remain the same. This conclusion leads to the seeming paradox that if c_{11} decreases then symmetry requires that c_{12} must increase which appears to contradict the fact that internal displacements must always lower the energy. The resolution of this seeming paradox comes from the fact that it is not possible to construct a strain in which c_{12} appears as the sole coefficient in the expression for the strain energy. It always appears in conjunction with c_{11} and we have already seen that $c_{11} + c_{12}$ is required by symmetry to be unchanged while $c_{11} - c_{12}$ can either decrease or remain unchanged.

Our results for the six independent and non-zero elastic constants of α -Pt₂Si are given in Table X. We have calculated the elastic constants for the “frozen” configuration [all atoms held at the positions determined solely from Eq. (3)] and with the relaxation of the strain-induced forces on the Pt atoms. In keeping with our general symmetry arguments, we find a relaxation-induced softening of c_{11} by 4% and of c_{44} by 17%. In addition, c_{12} increases by 6% while the remaining elastic constants are unchanged to within numerical uncertainties. Our results are also consistent with the symmetry requirement that the changes in c_{11} and c_{12} be equal and opposite, since c_{11} decreases by 14.8 ± 1.5 GPa whereas c_{12} increases by 14.6 ± 1.6 GPa. The bulk moduli calculated from the tetragonal elastic constants and from the fit to a Birch-Murnaghan equation of state are almost the same, giving a consistent prediction of $B_0 = 235$ GPa. As required by symmetry, the bulk modulus has the same value in the frozen and relaxed calculations.

The requirement that the crystal be stable against any homogeneous elastic deformation places restrictions on the elastic constants, just as in the cubic case. For tetragonal crystals these mechanical stability restrictions are as follows²⁴

$$\begin{aligned} (c_{11} - c_{12}) &> 0, & (c_{11} + c_{33} - 2c_{13}) &> 0, \\ c_{11} &> 0, & c_{33} &> 0, & c_{44} &> 0, & c_{66} &> 0, \\ (2c_{11} + c_{33} + 2c_{12} + 4c_{13}) &> 0. \end{aligned} \quad (13)$$

The elastic constants in Table X satisfy all of the conditions in Eq. (13). In particular, c_{12} is smaller than c_{11} and c_{13} is smaller than the average of c_{11} and c_{33} . The stability conditions again lead to restrictions on the magnitude of B_0 . We first rewrite B_0 as

$$B_0 = \frac{1}{9} [6c_{11} + 3c_{33} - 2(c_{11} - c_{12}) - 2(c_{11} + c_{33} - 2c_{13})]. \quad (14)$$

Using Eq. (14) and the first two inequalities in Eq. (13), we obtain the following result

$$B_0 < \frac{1}{3}(2c_{11} + c_{33}), \quad (15)$$

that the bulk modulus must be smaller than the weighted average of c_{11} and c_{33} . Similarly, by substituting instead

for c_{11} and c_{33} we obtain

$$B_0 > \frac{1}{3}(c_{12} + 2c_{13}), \quad (16)$$

that the bulk modulus must be larger than the weighted average of c_{12} and c_{13} .

The stability restrictions do not tell us anything further about the relative magnitudes of the various elastic constants. For example, we find a small value of c_{44} in comparison to c_{66} which means that the tetragonal unit cell is more easily deformed by a pure shear about the **a**- or **b**-axis in comparison to the **c**-axis. We also find that overall the elastic constants of α -Pt₂Si are much closer to those of pure Pt than pure Si. In particular c_{11} and c_{33} are similar in magnitude to c_{11} in Pt, but all of these constants are approximately twice the value of c_{11} in Si. Similarly c_{12} has approximately the same magnitude for both α -Pt₂Si and Pt, although c_{13} in the silicide is about 30% smaller. However, c_{12} in Si is a factor of four smaller. Conversely, the value of c_{44} is similar in magnitude for all three materials, with c_{66} in the silicide being a factor of two larger. The bulk modulus in the silicide is about 20% smaller than in Pt but still more than a factor of two larger than in Si. The connection between the magnitudes of the various elastic constants and the chemical bonding has been explored in detail in a separate study.³²

In addition to the relaxed elastic constants we also obtained the values of the dimensionless parameters $\zeta_i^{(I)}$ which determine the magnitudes of the Pt internal displacements themselves,

$$\Delta u_i^{(I)} = a \zeta_i^{(I)} \gamma, \quad (17)$$

where a is the lattice constant, $I = 1, 4, 6$ corresponds to the strains with symmetry-allowed internal displacements, and i is the Cartesian index ($i = 2, 3$ for $I = 6$ and $i = 3$ for $I = 1, 4$). In principle there could be contributions to the $\Delta u_i^{(I)}$ which are of higher order in γ , but since we are only considering the second order elastic constants the strain energy is only expanded to second order in γ [see Eqs. (5) and (8)], or equivalently, to second order in the total displacements, $u_i + \Delta u_i$. Thus we need only consider the linear term in Eq. (17) in the present context. The calculated values of the $\zeta_i^{(I)}$ parameters are listed in Table XI along with the displacement parameter associated with c_{44} in Si. We note that although displacements are allowed along both the [010] and [001] directions in the case of the α -Pt₂Si strain 6 (corresponding to c_{44}), the displacements along [001] are found to be zero to linear order in γ .³³ As indicated above, we expect the internal displacements for strains 1 and 4 to exhibit a symmetry-required relationship and in keeping with this expectation we find that $\zeta_3^{(I=1)}$ is almost exactly three times larger than $\zeta_3^{(I=4)}$, the difference likely being due to numerical uncertainty.

E. PtSi

Nine independent strains are necessary to compute the elastic constants of orthorhombic PtSi. We first performed calculations of the elastic constants with the internal structural parameters $u_{\text{Pt/Si}}$ and $v_{\text{Pt/Si}}$ held “frozen” at their self-consistent equilibrium values. These results are listed in the second column of Table XII. The $E(\gamma)$ curves are well-fitted by third-order polynomials in γ , as can be seen from the small standard errors in the calculated c_{ij} . The value of B_0 obtained from the elastic constants, $B_0 = \frac{1}{9}(c_{11} + c_{22} + c_{33} + 2c_{12} + 2c_{13} + 2c_{23})$, agrees reasonably well with the one which was determined from the calculation of the lattice constants. This is not surprising since the lattice constant calculations were also performed with frozen atomic degrees of freedom.

As expected, the equilibrium atomic positions are not independent of the shape and size of the unit cell—similarly to the case of c_{44} in Si as well as c_{11} , c_{12} , and c_{44} in α -Pt₂Si, as discussed above. The relaxed elastic constants for PtSi are listed in the last column of Table XII. For example, c_{44} drops from 141.3 GPa to 100.1 GPa when all of the atoms are relaxed. We find that the Si atoms adjust to this shear about the **a**-axis by moving mainly along the **b**-axis. Most of the other elastic constants decrease by 10–20%, except c_{23} which increases by 8% and c_{12} which remains approximately unchanged. In analogy with the case of c_{12} for tetragonal α -Pt₂Si, we note that for an arbitrary strain c_{12} , c_{13} , and c_{23} in orthorhombic PtSi never appear isolated but always occur in combination with other elastic constants in the expression for the second-order change in the total energy [Eq. (8)]. These particular elastic constants are therefore not required to decrease when relaxation is included, even when the energy is lowered. Conversely, the remaining six elastic constants *are* required to decrease when relaxation lowers the energy because strains can be constructed for which each appears as the isolated coefficient of the only contribution to the second-order change in the energy. In the case of PtSi, the additional relaxation of the internal degrees of freedom leads to a significant softening of the elastic constants which must also be taken into account in determining the bulk modulus. Therefore, we predict the bulk modulus of PtSi to be 198 GPa, which is 6% lower than the value of 210 GPa determined in our frozen-configuration total-energy minimization. Although we have calculated the changes in the elastic constants when the internal atomic degrees of freedom are allowed to relax, we have not explicitly extracted the corresponding internal displacement parameters as we did for pure Si and α -Pt₂Si.

Mechanical stability leads to restrictions on the elastic constants, which for orthorhombic crystals are as

follows²⁴

$$\begin{aligned} (c_{11} + c_{22} - 2c_{12}) &> 0, & (c_{11} + c_{33} - 2c_{13}) &> 0, \\ (c_{22} + c_{33} - 2c_{23}) &> 0, \\ c_{11} > 0, & c_{22} > 0, & c_{33} > 0, \\ c_{44} > 0, & c_{55} > 0, & c_{66} > 0, \\ (c_{11} + c_{22} + c_{33} + 2c_{12} + 2c_{13} + 2c_{23}) &> 0. \end{aligned} \quad (18)$$

The elastic constants in Table XII satisfy all of these conditions and in particular, c_{12} is smaller than the average of c_{11} and c_{22} , c_{13} is smaller than the average of c_{11} and c_{33} , and c_{23} is smaller than the average of c_{22} and c_{33} . As in the case of α -Pt₂Si, we can obtain restrictions on the magnitude of B_0 ,

$$\frac{1}{3}(c_{12} + c_{13} + c_{23}) < B_0 < \frac{1}{3}(c_{11} + c_{22} + c_{33}), \quad (19)$$

that the bulk modulus must be smaller than the average of c_{11} , c_{22} , and c_{33} but larger than the average of c_{12} , c_{13} , and c_{23} .

We again find that overall the elastic constants of PtSi are much closer to those of pure Pt and α -Pt₂Si as compared to pure Si. In detail, we find that c_{11} , c_{22} , and c_{33} are approximately 10% smaller on average in PtSi than in α -Pt₂Si, and that B_0 is 16% smaller. In addition, c_{12} , c_{13} , and c_{23} for PtSi are close in magnitude to c_{13} for α -Pt₂Si, which we saw was about 30% smaller than c_{12} in both pure Pt and α -Pt₂Si. Finally, c_{44} , c_{55} , and c_{66} for PtSi are similar to the values of c_{44} in all three of the other materials, but still approximately a factor of two smaller than c_{66} in α -Pt₂Si.

F. Trends in the elastic constants

The trends of the elastic constants as a function of the atomic percent Pt in all four materials are plotted in Fig. 2. Each of the curves corresponds to an average of a different class of elastic constants, while the symbols show the values of the individual elastic constants themselves. As we saw in Eqs. (15), (16), and (19), mechanical stability requires that B_0 be larger than the average of c_{11} , c_{22} , and c_{33} but smaller than the average of c_{12} , c_{13} , and c_{23} (note that in the case of α -Pt₂Si the appropriate averages are $\frac{1}{3}(2c_{11} + c_{33})$ and $\frac{1}{3}(c_{12} + 2c_{13})$ because $c_{11} = c_{22}$ and $c_{13} = c_{23}$ for tetragonal crystals). This stability requirement is reflected in the top three curves in Fig. 2. We also see that these three curves each increase monotonically from Si to Pt and we note that all three classes of elastic constants represented by these curves correspond to strains in which the volume is not fixed. Conversely, the two lower curves labeled $(c_{11} - c_{12})/2$ and c_{44} correspond to the two classes of elastic constants in which the strains are strictly volume-conserving [in the case of PtSi the lowest solid-line curve and large open circles correspond to elastic constant combinations $\frac{1}{4}(c_{11} + c_{22} - 2c_{12})$, $\frac{1}{4}(c_{11} + c_{33} - 2c_{13})$, and

$\frac{1}{4}(c_{22} + c_{33} - 2c_{23})$]. We see that in this case the two sets of averages are approximately constant as a function of atomic percent Pt. The significance of this difference in the trends of volume-conserving versus non-volume-conserving elastic constants is connected to the nature of the chemical bonding in these materials and has been addressed in a separate study.³²

IV. ELECTRONIC STRUCTURE

The self-consistent calculations for the spin-orbit-split energy bands of α -Pt₂Si and PtSi were performed using the WIEN97 implementation³⁴ of the linear augmented plane wave (LAPW) method.^{35,36} The local density approximation was used with the exchange-correlation potential of Perdew and Wang.³⁷ The effects of the spin-orbit interaction were included in a second-order variational procedure.^{36,38} In the self-consistency cycles approximately 120 irreducible \mathbf{k} -points (1000 \mathbf{k} -points in the full BZ) were used in the modified tetrahedron method of Blöchl.³⁹ The energy cutoff used for the plane-wave expansion was $k_{\text{max}} = 4.16$ a.u. resulting in a well converged basis set of about 105 basis functions per atom. The experimental values of the lattice constants and internal structural parameters from Tables II and III were used in all cases. For the purpose of calculating the density of states (DOS) we again used the tetrahedron method but with unshifted \mathbf{k} -point meshes which included the Γ point. In the case of fcc Pt, cubic-diamond-phase Si, and α -Pt₂Si we used a $32 \times 32 \times 32$ mesh corresponding to 897 irreducible \mathbf{k} -points for the two cubic materials and 2393 for the silicide. For PtSi we used a $16 \times 24 \times 16$ mesh, yielding 1053 irreducible \mathbf{k} -points points.

The total DOS for all four materials is shown on the same scale in Fig. 3. Although both silicides are metals with a non-zero DOS at the Fermi level, they are found to be poor metals since the DOS is much smaller than in the case of pure Pt which is a good metal. In pure Pt the Fermi level lies near the top but still within the large DOS features of the d -band but in both silicides the Fermi level lies above these large peaks. In addition, both silicides exhibit a peak in the DOS at around -10 eV which arises from the Si s -orbitals. We note that the basic features of the electronic structure, as reflected in the total DOS, do not appear to differ very much between the two silicides. The origin of the various features in the PtSi DOS has been discussed in detail by Franco *et al.*⁴⁰

We have also calculated the spin-orbit-split energy bands near the Fermi level for the two silicides, as shown in Fig. 4. In both cases we see that there are a sizeable number of small-energy splittings between different bands throughout the full BZ. These small splittings are of direct interest with regard to low-energy inter-band transitions which contribute to the optical absorption.

In a typical good metal such as Pt, the optical absorption at low energies is dominated by the free-electron-like Drude contribution. However, we saw from Fig. 3 that in the case of the silicides they have a low DOS at the Fermi level and consequently are poor metals. In this circumstance the Drude contribution will be greatly reduced and therefore the presence of many low-energy splittings in the bands near the Fermi level may result in an inter-band contribution to the optical absorption which is significant even at low energies in the infrared range.

V. SUMMARY

We have carried out an extensive first principles study of two room-temperature stable Pt silicides, tetragonal α -Pt₂Si and orthorhombic PtSi. We have determined the theoretical equilibrium structural parameters and cohesive energies for both silicides, as well as pure fcc Pt and pure cubic-diamond-phase Si. In particular, we have carried out a large number of calculations in order to minimize the total energy with respect to the two lattice constants in tetragonal α -Pt₂Si and the three lattice constants and four internal structural parameters of orthorhombic PtSi. Our calculated structural parameters for all four materials are in good agreement with experimental data, validating the method we have used.

A major portion of our effort here has been directed at the elastic constants in the two silicides. All of the independent, non-zero elastic constants (6 for α -Pt₂Si, 9 for PtSi, and 3 each for the two cubic materials) have been calculated from first principles. The silicide calculations required extensive relaxation of the internal degrees of freedom, especially in the case of the low symmetry structure of orthorhombic PtSi. Comparing the elastic constants obtained with and without relaxation we find that relaxation induces significant changes in the magnitudes of many of the elastic constants. In addition, we have explicitly determined the dimensionless internal displacement parameters for the three strains in α -Pt₂Si for which they are non-zero. We also note that the value of c_{44} in pure fcc Pt was found to be extremely sensitive to the number of \mathbf{k} -points, much more so than any of the other elastic constants we calculated. This sensitivity results from the large number of van Hove singularities close to the Fermi level.

We have investigated the trends in the calculated elastic constants, both the trends within a given material as well as between materials. The requirement of mechanical stability places specific restrictions on the relative magnitudes of some of the elastic constants within a given material, including, for example, a restriction on the bulk modulus that $B_0 < \frac{1}{3}(c_{11} + c_{22} + c_{33})$ and $B_0 > \frac{1}{3}(c_{12} + c_{13} + c_{23})$. With regard to the trends among the four materials, we find that in the metals the elastic constant expressions which correspond to volume-

conserving strains are always smaller than those which correspond to strains which do not conserve volume. This also turns out to be true in Si with the exception of c_{12} which is less than c_{44} . However, the difference in magnitudes between volume-conserving and non-volume-conserving elastic constants is largest on average in Pt and gets smaller in the progression $\text{Pt} \rightarrow \alpha\text{-Pt}_2\text{Si} \rightarrow \text{PtSi} \rightarrow \text{Si}$. In general, the volume-conserving elastic constants have similar magnitudes in all four materials while the non-volume-conserving elastic constants follow this same progression. In particular, the bulk modulus is found to be a very nearly linear function of the atomic percentage of Pt. Klepeis *et al.*³² have studied the close connection between the various trends in the elastic constants and the chemical bonding in the Pt silicides.

The calculated electronic structure demonstrates that the two silicides are poor metals with a low density of states at the Fermi level, and consequently we expect that the Drude component of the optical absorption should be much smaller than in good metals such as pure Pt. In addition, we find a large number of small-energy differences between various bands near the Fermi level in the calculated spin-orbit-split band structure for the two silicides. These two circumstances suggest that it may be important to include the interband contribution to the optical absorption as well, even in the infrared region.

ACKNOWLEDGMENTS

This work was performed in part under the auspices of the U. S. Department of Energy, Office of Basic Energy Sciences, Division of Materials Science by the University of California Lawrence Livermore National Laboratory under contract No. W-7405-Eng-48. Partial support was also provided by Deutsche Forschungsgemeinschaft, SFB 292 "Multicomponent Layered Systems."

¹ V. W. Chin, M. A. Green, and J. W. V. Storey, *Solid-State Electron.* **36**, 1107 (1993).

² P. W. Pellegrini, C. E. Ludington, and M. M. Weeks, *J. Appl. Phys.* **67**, 1417 (1990).

³ P. W. Pellegrini, A. Golubovic, C. E. Ludington, and M. M. Weeks, *International Electron Devices Meeting Technical Digest*, IEEE (New York, San Francisco, CA, USA, 1982), pp. 157–60.

⁴ O. Bisi and C. Calandra, *J. Phys. C* **14**, 5479 (1981).

⁵ Y. M. Yarmoshenko, S. N. Shamin, L. V. Elokhina, V. E. Dolgih, E. Z. Kurmaev, S. Bartkowski, M. Neumann, D. L. Ederer, K. Göransson, B. Nöläng, and I. Engström, *J. Phys.: Condens. Matter* **9**, 9403 (1997).

⁶ W. B. Pearson, *A Handbook of Lattice Spacings and Structures of Metals and Alloys*, Vol. 4 of *International Series*

of Monographs on Metal Physics and Physical Metallurgy, edited by G. V. Raynor (Pergamon Press, Oxford, 1964).

⁷ *Semiconductors: Group IV Elements and III–V Compounds*, Vol. 17a *Landolt-Börnstein, New Series, Group III*, edited by O. Madelung (Springer, Berlin, 1982).

⁸ R. P. Ram and S. Bhan, *Z. Metallkde.* **69**, 524 (1978).

⁹ R. Gohle and K. Schubert, *Z. Metallkde.* **55**, 503 (1964).

¹⁰ H. Pfisterer and K. Schubert, *Z. Metallkde.* **41**, 358 (1950).

¹¹ E. J. Graeber, R. J. Baughman, and B. Morosin, *Acta Cryst. B* **29**, 1991 (1973).

¹² M. Methfessel, *NFP Manual*, Institute for Semiconductor Physics, Frankfurt (Oder), 1997.

¹³ M. Methfessel, M. van Schilfgaarde, and R. A. Casali, in *Electronic Structure and Physical Properties of Solids: The Uses of the LMTO Method, Lecture Notes in Physics*, Workshop Mont Saint Odile, France 1998, edited by H. Dreyse (Springer, Berlin 2000).

¹⁴ E. Bott, M. Methfessel, W. Krabs, and P. C. Schmidt, *J. Math. Phys.* **39**, 3393 (1998).

¹⁵ D. M. Ceperley and B. J. Alder, *Phys. Rev. Lett.* **45**, 566 (1980).

¹⁶ The basis used here is "minimal" in the sense that removal of any one of the L -blocks listed in Table IV would result in a significant reduction in accuracy. However, we have tested this basis on the equilibrium lattice constants and elastic constants of pure Pt and pure Si (see Tables II and IX). For example, adding a third d -block for Pt results in only a 0.2% reduction in the theoretical equilibrium lattice constant.

¹⁷ F. D. Murnaghan, *Proc. Natl. Acad. Sci. USA* **30**, 244 (1944).

¹⁸ C.-L. Fu and K.-M. Ho, *Phys. Rev. B* **28**, 5480 (1983).

¹⁹ E. Birch, *J. Geophys. Res.* **83**, 1257 (1978).

²⁰ M. Methfessel and M. van Schilfgaarde, *Phys. Rev. B* **48**, 4937 (1993).

²¹ See for example, N. W. Ashcroft and N. D. Mermin, *Solid State Physics* (Saunders College, Philadelphia, 1976), Chap. 22, pp. 425–6.

²² Alternatively, one could take geometry relaxations into account while simultaneously varying the lattice constants, but this approach is computationally demanding. Nevertheless, this method was required for the elastic constant calculations discussed in Sec. III A, as demonstrated by the considerable differences between "frozen" and "relaxed" elastic constants (see Tables X and XII).

²³ J. F. Nye, *Physical Properties of Crystals*, (Oxford University Press, Oxford, 1985).

²⁴ D. C. Wallace, *Thermodynamics of Crystals* (John Wiley & Sons, New York, 1972), Chap. 1, where finite Lagrangian strains η_{ij} are discussed. In the case of infinitesimal strains these reduce to our ϵ_{ij} of classical elasticity theory.⁴¹

²⁵ M. J. Mehl, J. E. Osburn, D. A. Papaconstantopoulos, and B. M. Klein, *Phys. Rev. B* **41**, 10311 (1990), and erratum [*Phys. Rev. B* **42**, 5362 (1990)].

²⁶ We could also have used a simpler strain 3 in Table VII in order to determine c_{66} , namely $e_6 = 2\gamma$ with $\Delta E/V = 2c_{66}\gamma^2$.

²⁷ M. Alouani, R. C. Albers, and M. Methfessel, *Phys. Rev. B* **43**, 6500 (1991).

²⁸ R. E. MacFarlane, J. A. Rayne, and C. K. Jones,

- Phys. Lett. **18**, 91 (1965).
- ²⁹ M. Methfessel and A. T. Paxton, Phys. Rev. B **40**, 3616 (1989).
- ³⁰ *Low Frequency Properties of Dielectric Crystals*, Vol. 29a *Landolt-Börnstein, New Series, Group III*, edited by D. F. Nelson (Springer, Berlin, 1992).
- ³¹ C. S. G. Cousins, L. Gerward, J. S. Olsen, B. Selsmark, and B. J. Sheldon, J. Phys. C **20**, 29 (1987).
- ³² J. E. Klepeis, O. Beckstein, G. L. W. Hart, and O. Pankratov, Phys. Rev. B (submitted).
- ³³ The calculated displacements along [001] for strain 6 are found to be approximately a factor of 30 smaller than the displacements along [010] and they do not depend on the sign but only the magnitude of γ .
- ³⁴ P. Blaha, K. Schwarz, and J. Luitz, WIEN97, Vienna University of Technology, 1997, updated version of Ref. 42.
- ³⁵ O. K. Andersen, Phys. Rev. B **12**, 3060 (1975).
- ³⁶ D. J. Singh, *Planewaves, Pseudopotentials and the LAPW Method* (Kluwer Academic Publishers, Boston, 1994).
- ³⁷ J. P. Perdew and Y. Wang, Phys. Rev. B **44**, 13 244 (1992).
- ³⁸ P. Novak, unpublished (1997).
- ³⁹ P. E. Blöchl, O. Jepsen, and O. K. Andersen, Phys. Rev. B **49**, 16 223 (1994).
- ⁴⁰ N. Franco, J. Klepeis, C. Bostedt, A. Van Buuren, C. Heske, O. Pankratov, T. Calcott, E. Ederer, and L. J. Terminello, (to be published).
- ⁴¹ F. Birch, Phys. Rev. **71**, 809 (1947).
- ⁴² P. Blaha, K. Schwarz, P. Sorantin, and S. B. Trickey, Comp. Phys. Comm. **59**, 399 (1990).
- ⁴³ C. Kittel, *Introduction to Solid State Physics*, 6th ed., (Wiley, New York, 1986).
- ⁴⁴ L. Topor and O. J. Kleppa, Z. Metallkde. **77**, 65 (1986).
- ⁴⁵ M. S. Chandrasekharaiah, J. L. Margrave, and P. A. G. O'Hare, J. Phys. Chem. Ref. Data **22**, 1459 (1993).
- ⁴⁶ *International Tables for Crystallography*, Vol. A *Space-Group Symmetry*, 2nd ed., edited by T. Hahn (Kluwer Academic, Dordrecht, 1989).
- ⁴⁷ P. Villars and L. D. Calvert, *Pearson's Handbook of Crystallographic Data for Intermetallic Phases* (ASM International, Materials Park, 1991), Vol. 4, p. 4994.
- ⁴⁸ *Structure Data of Elements and Intermetallic Phases*, Vol. 6 *Landolt-Börnstein, New Series, Group III*, edited by K.-H. Hellwege (Springer, Berlin, 1971).
- ⁴⁹ The “experimental” cohesive energy for α -Pt₂Si was calculated as $E_{\text{coh}} = \frac{2}{3}E_{\text{coh}}(\text{Pt}) + \frac{1}{3}E_{\text{coh}}(\text{Si}) - \Delta H_{\text{f}}^{298.15}(\alpha\text{-Pt}_2\text{Si})$ from the experimental cohesive energies⁴³ and the molar heat of formation,⁴⁴ without correcting for the difference between 298.15 and 0 K.
- ⁵⁰ The “experimental” cohesive energy for PtSi was calculated as $E_{\text{coh}} = \frac{1}{2}E_{\text{coh}}(\text{Pt}) + \frac{1}{2}E_{\text{coh}}(\text{Si}) - \Delta H_{\text{f}}^{298.15}(\text{PtSi})$ from the experimental cohesive energies⁴³ and the molar heat of formation,⁴⁵ without correcting for the difference between 298.15 and 0 K.

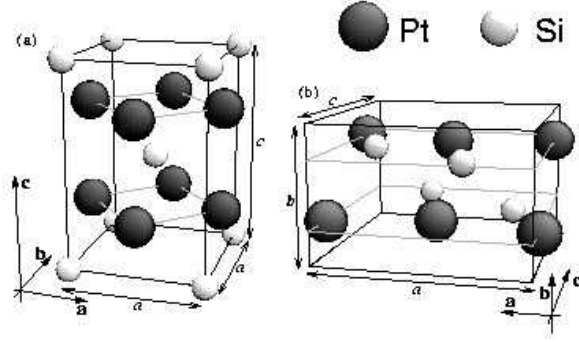


FIG. 1. Conventional unit cells of (a) body-centered tetragonal α -Pt₂Si and (b) orthorhombic PtSi. The relevant lattice constant distances are illustrated in both cases.

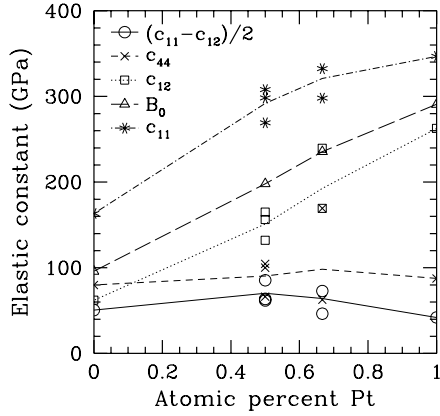


FIG. 2. Trends in the elastic constants as a function of atomic percent Pt for pure cubic-diamond-phase Si, orthorhombic PtSi, tetragonal α -Pt₂Si, and fcc Pt. The different curves correspond to the average values of different classes of the individual elastic constants, as specified in the legend. For example, in the case of the dotted-line curve labeled as c_{12} , the line passes through $\frac{1}{3}(c_{12} + c_{13} + c_{23})$ in the case of PtSi and through $\frac{1}{3}(c_{12} + 2c_{13})$ for α -Pt₂Si ($c_{13} = c_{23}$ for tetragonal crystals), while the open squares show the actual values of c_{12} , c_{13} and c_{23} , as appropriate for each material.

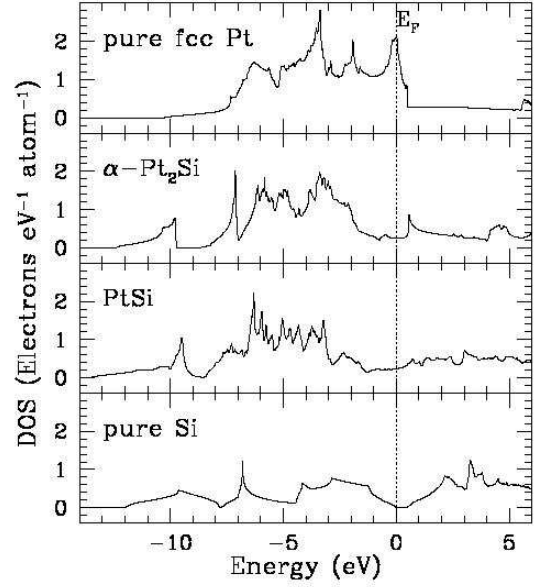


FIG. 3. Total density of states plotted on the same scale for the four materials considered in this work, ordered by decreasing Pt content from top to bottom. Only Si is a semiconductor whereas Pt and the two silicides are metals. The valence band maximum in Si is labeled as the Fermi level E_F .

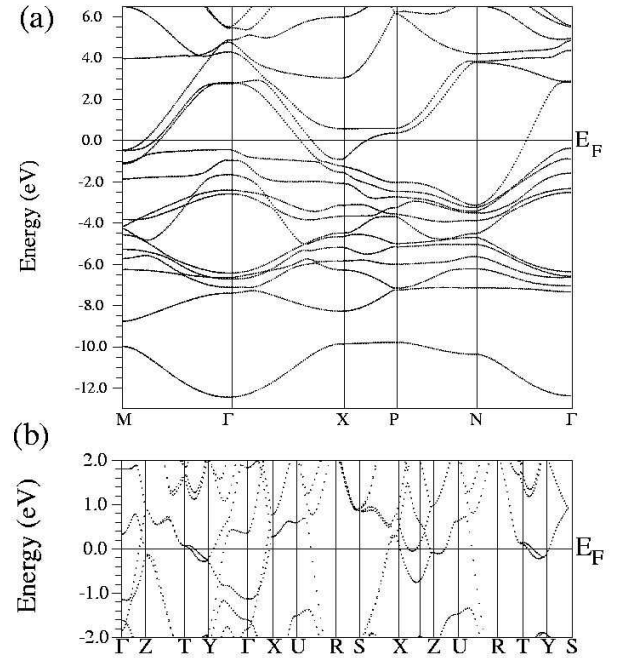


FIG. 4. Spin-orbit split energy bands near the Fermi level for (a) α -Pt₂Si and (b) PtSi. The primary feature of interest in both plots is the relatively large number of low-energy splittings between various bands near the Fermi level.

TABLE I. Structural characterization of the materials studied in this work. The column labeled “Structure” gives the Strukturbericht designations. The columns “Space Group” (name and number), “Site” (multiplicity and Wyckoff letter), and “1st position” follow Ref. 46. See Table III for the values of the internal structural parameters u and v .

Material	Structure	Space group		Site		1st position	Ref.
Pt	$A1$	$Fm\bar{3}m$	225	Pt	$4a$	0, 0, 0	6
α -Pt ₂ Si	$L'2_b$	$I4/mmm$	139	Pt	$4d$	$0, \frac{1}{2}, \frac{1}{4}$	8
				Si	$2a$	0, 0, 0	
PtSi	$B31$	$Pnma$	62	Pt	$4c$	$u_{\text{Pt}}, \frac{1}{4}, v_{\text{Pt}}$	11,47
				Si	$4c$	$u_{\text{Si}}, \frac{1}{4}, v_{\text{Si}}$	
Si	$A4$	$Fd\bar{3}m$	227	Si	$8a$	$\frac{1}{8}, \frac{1}{8}, \frac{1}{8}$	7

TABLE II. Theoretical and experimental lattice constants (in a.u.) and bulk moduli B_0 (in GPa). The theoretical B_0 were determined from a fit to a Murnaghan equation of state for Pt and Si, and to a four-term Birch-Murnaghan equation of state for α -Pt₂Si and PtSi. B_0 listed here for PtSi was calculated for fixed values of the internal structural parameters (see also Table XII). The experimental value of the bulk modulus for Pt is extrapolated to 0 K, whereas all of the other experimental numbers are given for room temperature.

Material		a_0	b_0	c_0	B_0	Ref.
Pt	theor.	7.403			287.8	
	exp.	7.415			288.4	48,28
α -Pt ₂ Si	theor.	7.407		11.241	233.5	
	exp.	7.461		11.268	—	8
PtSi	theor.	10.583	6.774	11.195	210.0	
	exp.	10.539	6.778	11.180	—	11
Si	theor.	10.22			95.9	
	exp.	10.26			98.8	30

TABLE III. Calculated and experimental internal structural parameters of PtSi. The parameters u and v are the same as those specified in Table I. These parameters were calculated both for the experimental lattice constants as well as the self-consistent theoretical lattice constants (Table II). The experimental internal parameters for PtSi are also listed.

PtSi	u_{Pt}	v_{Pt}	u_{Si}	v_{Si}
At expt. lattice constants	0.9981	0.1915	0.1777	0.5845
At theor. lattice constants	0.9977	0.1919	0.1782	0.5841
Experiment ¹¹	0.9956	0.1922	0.177	0.583

TABLE IV. Parameters describing the basis used in the FPLMTO calculations. R_{mt} is the muffin-tin radius in a.u., L_{max} is the upper limit on the angular momentum expansion of the smoothed Hankel functions about a given atomic site, K_{max} is the order of the biorthogonal polynomials used in this expansion, R_{sm} is the smoothing radius in a.u., and $-\kappa^2$ is the decay energy. The total number of basis functions per atom is 17 for Pt and 13 for Si. See Ref. 12 for a more complete description of the parameters.

Atom	R_{mt}	L_{max}	K_{max}	L -Block	Basis R_{sm}	$-\kappa^2$
Pt	2.2	3	4	s	2.865	-1.02
				p	2.130	-1.08
				p	1.302	-1.53
				d	1.000	-0.89
				d	2.123	-0.42
Si	2.1	3	5	s	1.908	-1.296
				p	1.627	-0.302
				d	1.601	-1.496
				s,p	2.200	-2.000

TABLE V. Cohesive energies E_{coh} and heats of formation ΔH_{f} in eV/atom. The experimental standard heat of formation is given for $T = 298.15$ K whereas theoretical values are valid for 0 K and do not contain any corrections for zero-point vibrations. The experimental cohesive energies for Pt and Si also correspond to 0 K.

Material		E_{coh}	ΔH_{f}	Ref.
Pt	theor.	7.27	0	
	exp.	5.84	0	43
α -Pt ₂ Si	theor.	7.24	-0.65	
	exp.	6.08	-0.64	44,49
PtSi	theor.	6.93	-0.67	
	exp.	5.85	-0.62	45,50
Si	theor.	5.23	0	
	exp.	4.63	0	43

TABLE VI. Parameterizations of the three strains used to calculate the three elastic constants of cubic Pt and Si (also used in Ref. 25). The energy expressions were obtained from Eq. (8). Strains $I = 1$ and $I = 3$ are strictly volume-conserving to all orders in the strain parameter γ . If we restrict ourselves to linear order only then $e_3^{(1)} = -2\gamma$ and $e_3^{(3)} = 0$, with volume conservation preserved to linear order as well.

Strain I	Parameters (unlisted $e_i = 0$)	$\Delta E/V$ to $O(\gamma^2)$
1	$e_1 = e_2 = \gamma, e_3 = (1 + \gamma)^{-2} - 1$	$3(c_{11} - c_{12})\gamma^2$
2	$e_1 = e_2 = e_3 = \gamma$	$\frac{3}{2}(c_{11} + 2c_{12})\gamma^2$
3	$e_6 = \gamma, e_3 = \gamma^2(4 - \gamma^2)^{-1}$	$\frac{1}{2}c_{44}\gamma^2$

TABLE VII. Parameterizations of the six strains used to calculate the six elastic constants of tetragonal α -Pt₂Si (taken from Ref. 27). The energy expressions were obtained from Eq. (8).

Strain I	Parameters (unlisted $e_i = 0$)	$\Delta E/V$ to $O(\gamma^2)$
1	$e_1 = 2\gamma, e_2 = e_3 = -\gamma$	$\frac{1}{2}(5c_{11} - 4c_{12} - 2c_{13} + c_{33})\gamma^2$
2	$e_1 = e_2 = -\gamma, e_3 = 2\gamma$	$(c_{11} + c_{12} - 4c_{13} + 2c_{33})\gamma^2$
3	$e_1 = e_2 = \gamma, e_3 = -2\gamma, e_6 = 2\gamma$	$(c_{11} + c_{12} - 4c_{13} + 2c_{33} + 2c_{66})\gamma^2$
4	$e_1 = \gamma$	$\frac{1}{2}c_{11}\gamma^2$
5	$e_3 = \gamma$	$\frac{1}{2}c_{33}\gamma^2$
6	$e_4 = 2\gamma$	$2c_{44}\gamma^2$

TABLE VIII. Parameterizations of the nine strains used to calculate the nine elastic constants of orthorhombic PtSi. The energy expressions were obtained from Eq. (8).

Strain I	Parameters (unlisted $e_i = 0$)	$\Delta E/V$ to $O(\gamma^2)$
1	$e_1 = \gamma$	$\frac{1}{2}c_{11}\gamma^2$
2	$e_2 = \gamma$	$\frac{1}{2}c_{22}\gamma^2$
3	$e_3 = \gamma$	$\frac{1}{2}c_{33}\gamma^2$
4	$e_1 = 2\gamma, e_2 = -\gamma, e_3 = -\gamma$	$\frac{1}{2}(4c_{11} - 4c_{12} - 4c_{13} + c_{22} + 2c_{23} + c_{33})\gamma^2$
5	$e_1 = -\gamma, e_2 = 2\gamma, e_3 = -\gamma$	$\frac{1}{2}(c_{11} - 4c_{12} + 2c_{13} + 4c_{22} - 4c_{23} + c_{33})\gamma^2$
6	$e_1 = -\gamma, e_2 = -\gamma, e_3 = 2\gamma$	$\frac{1}{2}(c_{11} + 2c_{12} - 4c_{13} + c_{22} - 4c_{23} + 4c_{33})\gamma^2$
7	$e_4 = \gamma$	$\frac{1}{2}c_{44}\gamma^2$
8	$e_5 = \gamma$	$\frac{1}{2}c_{55}\gamma^2$
9	$e_6 = \gamma$	$\frac{1}{2}c_{66}\gamma^2$

TABLE IX. Elastic constants of Pt and Si. Calculations were carried out at the theoretical self-consistent lattice constants of $a_{\text{Pt}} = 7.403$ a.u. and $a_{\text{Si}} = 10.22$ a.u. The theoretical value of c_{44} in parentheses for Si is the “frozen” value obtained without allowing for internal relaxation. The bulk modulus is calculated from the elastic constants as $B_0 = \frac{1}{3}(c_{11} + 2c_{12})$. In parentheses we give B_0 from the fit to a Murnaghan equation of state. Experimental values are extrapolated to 0 K. All values are in units of GPa.

	Pt Theory	Pt Expt. ²⁸	Si Theory	Si Expt. ³⁰
c_{11}	346.8±0.5	358	163.45±0.03	165
c_{12}	262.7±0.3	254	62.13±0.02	63
c_{44}	87.5±0.3	77	79.85±0.02 (108.6)	79.1
B_0	290.8±0.3 (287.8)	288.4	95.90±0.02 (95.9)	97.0

TABLE X. Elastic constants of α -Pt₂Si. Calculations were performed at the theoretical self-consistent lattice constants (Table II). “Frozen” refers to fixed atomic positions, whereas “relaxed” indicates that a relaxation of the atomic positions was carried out. Parentheses denote values where no internal relaxation was necessary because of symmetry constraints (small variations in these values come from using a slightly more stringent convergence criterion on the energy). The bulk modulus is calculated from the elastic constants as $B_0 = \frac{1}{9}(2c_{11} + c_{33} + 2c_{12} + 4c_{13})$. B_0^{Birch} is from a Birch-Murnaghan fit. No experimental data is available. All values are in units of GPa.

α -Pt ₂ Si	frozen	relaxed
c_{11}	347.2±1.2	332.4±0.9
c_{33}	297.5±0.5	(298.0±0.4)
c_{12}	225.0±1.2	239.6±1.0
c_{13}	169.3±0.9	(169.4±0.8)
c_{44}	75.4±0.3	62.7±0.5
c_{66}	169.5±5.2	(169.3±5.2)
B_0	235.4±0.6	(235.5±0.5)
B_0^{Birch}	233.5	—

TABLE XI. Dimensionless internal displacement parameters ζ for Si [Eq. (12), strain 3 from Table VI] and α -Pt₂Si [Eq. (17), strains 1, 4, and 6 from Table VII]. In the case of strain 6 for α -Pt₂Si displacements were calculated along both the [010] and [001] directions, whereas displacements only along the [001] direction are allowed by symmetry for strains 1 and 4. In addition, there is a strict symmetry-required relationship between the displacements in strains 1 and 4 (see text). Experimental data is available only for Si.

Material	Strain I	Theory	Experiment	Ref.
Si	3	0.53	0.54	31
α -Pt ₂ Si	1	0.22	—	
	4	0.074	—	
	6 [010]	−0.12	—	
	6 [001]	0.00	—	

TABLE XII. Elastic constants of PtSi calculated at the theoretical self-consistent lattice constants (Table II). The second column shows the elastic constants obtained when the internal structural parameters were held fixed at their theoretical self-consistent values (Table III). In the third column these were allowed to relax. The bulk modulus is calculated from the elastic constants as $B_0 = \frac{1}{9}(c_{11} + c_{22} + c_{33} + 2c_{12} + 2c_{13} + 2c_{23})$. B_0^{Birch} is from a Birch-Murnaghan fit obtained with frozen values of the internal structural parameters. No experimental data is available. All values are in units of GPa.

PtSi	frozen	relaxed
c_{11}	327.5±1.2	298.2±1.2
c_{22}	313.8±0.0	269.3±0.8
c_{33}	345.9±0.1	308.0±0.6
c_{12}	157.7±0.6	156.4±0.8
c_{13}	162.9±0.6	132.2±0.7
c_{23}	153.4±0.1	165.1±0.6
c_{44}	141.3±0.3	100.1±0.4
c_{55}	113.1±0.1	104.5±0.1
c_{66}	74.2±0.2	66.3±0.4
B_0	215.0±0.2	198.1±0.3
B_0^{Birch}	210.0	—